



RESEARCH ARTICLE

10.1002/2015WR018095

Key Points:

- Defined hierarchy of land-surface factors' dominance on soil moisture
- Determined scale-specific variability in soil moisture
- Dominance of land-surface factors varies with hydroclimate

Correspondence to:

B. P. Mohanty,
bmohanty@tamu.edu

Citation:

Gaur, N., and B. P. Mohanty (2016), Land-surface controls on near-surface soil moisture dynamics: Traversing remote sensing footprints, *Water Resour. Res.*, 52, doi:10.1002/2015WR018095.

Received 16 SEP 2015

Accepted 31 JUL 2016

Accepted article online 5 AUG 2016

Land-surface controls on near-surface soil moisture dynamics: Traversing remote sensing footprints

Nandita Gaur¹ and Binayak P. Mohanty¹

¹Department of Biological and Agricultural Engineering, Texas A&M University, College Station, Texas, USA

Abstract In this new era of remote-sensing based hydrology, a major unanswered question is how to incorporate the impact of land-surface based heterogeneity on soil moisture dynamics at remote sensing scales. The answer to this question is complicated since (1) soil moisture dynamics that vary with support, extent, and spacing scales are dependent on land-surface based heterogeneity and (2) land-surface based heterogeneity itself is scale-specific and varies with hydroclimates. Land-surface factors such as soil, vegetation, and topography affect soil moisture dynamics by redistributing the available soil moisture on the ground. In this study, we determined the contribution of these biophysical factors to redistribution of near-surface soil moisture across a range of remote sensing scales varying from an (airborne) remote sensor footprint (1.6 km) to a (satellite) footprint scale (25.6 km). Two-dimensional nondecimated wavelet transform was used to extract the support scale information from the spatial signals of the land-surface and soil moisture variables. The study was conducted in three hydroclimates: humid (Iowa), subhumid (Oklahoma), and semiarid (Arizona). The dominance of soil on soil moisture dynamics typically decreased from airborne to satellite footprint scales whereas the influence of topography and vegetation increased with increasing support scale for all three hydroclimates. The distinct effect of hydroclimate was identifiable in the soil attributes dominating the soil moisture dynamics. The near-surface soil moisture dynamics in Arizona (semiarid) can be attributed more to the clay content which is an effective limiting parameter for evaporation whereas in Oklahoma (humid), sand content (limiting parameter for drainage) was the dominant soil attribute. The findings from this study can provide a deeper understanding of the impact of heterogeneity on soil moisture dynamics and the potential improvement of hydrological models operating at footprints' scales.

1. Introduction

Near-surface soil moisture dynamics refer to the variations in near surface soil moisture. Along with root zone soil moisture, they govern (1) partitioning of the energy and water budget, (2) triggers for runoff on the land surface or infiltration into the deeper layers after rainfall depending on the antecedent moisture conditions, (3) modulation of groundwater recharge rates and contaminant transport to the groundwater, and (4) bottom boundary condition for climate models and top boundary condition for watershed hydrology and agricultural production models. However, the apparent soil moisture dynamics vary widely with the spatial and temporal support, spacing, and extent scale of soil moisture measurements [Blöschl and Sivapalan, 1995; Gaur and Mohanty, 2013]. The advent of a remote sensing (RS) era in hydrology has led to increased availability of data over larger extents, coarse remote sensing supports (footprints), and regular spacing whereas our understanding of soil moisture dynamics (Richard's equation, Richard [1931]) has been based on soil moisture data collected at smaller extents, fine (of the order of a few centimeters) support scale and irregular spacing. In order to exploit the full potential of soil moisture estimation from space and enable transfer of knowledge of soil moisture dynamics between scales, it is essential to understand soil moisture dynamics from a remote sensing (support, spacing, and extent) scale perspective. Another important factor governing soil moisture dynamics at the RS footprint is the hydroclimate of the region. The hydroclimate of a region determines the amount of input water (in terms of precipitation) to any region and discounting tectonic activity or nature of parent rock material, it also represents the nature of landscape forming agents (like precipitation, temperature extremes observed in a region etc.). For example, an arid hydroclimate (like deserts) will be dry and will typically have poorly formed coarser sandy soils since a major weathering agent (water) is available in low quantity. Likewise, the vegetation density is also determined by

the precipitation amount, temperature etc. while many topographic features (rills etc.) may also be generated as a result of long-term impact of channeling of precipitation. Since soil type, vegetation (type, density etc.), topography, and precipitation history control soil moisture dynamics [Mohanty and Skaggs, 2001; Gaur and Mohanty, 2013], it can be hypothesized that dynamics of soil moisture are hydroclimate specific.

Past literature has focused extensively on understanding correlations between physical factors and soil moisture using geostatistics. This has enabled scientists to evaluate their effect on soil moisture at varying extent and spacing scales but fixed support scale. Only a few studies have discussed soil moisture variability by varying support scales and have mostly been limited by the scales and/or hydroclimates being analyzed. For the Southern Great Plains (SGP) region in Oklahoma, *Ryu and Famiglietti* [2006] used data at approximately $1 \text{ km} \times 1 \text{ km}$ to generate semivariograms of soil moisture. They scaled their semivariograms using “regularization” to make inferences for the semivariogram behavior at different support scales and attributed correlation lengths varying between 10 and 30 km to spatial patterns of soil texture while correlation lengths varying between 60 and 100 km to rainfall patterns for the 1 km support scale. The same was also suggested by *Kim and Barros* [2002] who used data at $800 \text{ m} \times 800 \text{ m}$ and *Oldak et al.* [2002] who used data at $400 \text{ m} \times 400 \text{ m}$ support in the SGP region. *Cosh and Brutsaert* [1999] used data at $200 \text{ m} \times 200 \text{ m}$ support scale and demonstrated a soil-based control on soil moisture distribution which was also corroborated by *Gaur and Mohanty* [2013] who used data at $800 \text{ m} \times 800 \text{ m}$. Over the same region, *Jawson and Niemann* [2007] used empirical orthogonal functions to demonstrate that the largest influence on soil moisture ($800 \text{ m} \times 800 \text{ m}$) was typically due to sand content except on the dry days where clay content played the dominant role. *Joshi and Mohanty* [2010] used data collected at the 800 m support scale in Iowa and argued that rainfall, topography, and soil texture have maximum effect on soil moisture distribution with limited influence of vegetation. Using data at finer support scale (i.e., collected using impedance probes, time domain reflectometry, and tensiometer-based probes), soil moisture distribution was also shown to be influenced by variable land cover, land management, microheterogeneity [Mohanty et al., 2000a], and topography [Mohanty et al., 2000b; Burt and Butcher, 1985; Western et al., 1999].

Considering the lack of and need for studies regarding the effect of varying support scales on the relationship between soil moisture and heterogeneity, the primary objective of this study was to determine the hierarchical dominance of land-surface (soil, vegetation, and topography) factors on soil moisture across remote sensing support scales varying from 1.6 km (airborne) to 25.6 km (satellite) for three hydroclimates. The extent and spacing scale for the study was fixed at regional extent (area $>2496 \text{ km}^2$) and regular spacing (0.8 km) while the support was varied to extract support scale specific information from the spatial signal of the physical variables using two-dimensional nondecimated wavelet transform. A number of attributes were chosen to represent soil, vegetation, and topography for a comprehensive evaluation of the land-surface factors. To the best of the authors’ knowledge, this is the first study addressing the physical controls of near-surface soil moisture across such a wide range of support scales.

2. Study Area and Data

2.1. Climatology

The study has been conducted using soil moisture data from the growing season of 1997, 2002, and 2004 in three different hydroclimates (Figure 1). The first region lies in Arizona. The climate in this region is classified as “arid-steppe-hot” (Köppen climate classification BSh, *Peel et al.* [2007], *Ackerman* [1941]). The annual mean precipitation of the region is $\sim 350 \text{ mm}$ as recorded in the town of Tombstone located within the study area. Over 60% of the total annual rainfall occurs during July–September as a result of the North American Monsoon in the form of localized, high intensity, and short convective thunderstorms [Ryu et al., 2010]. The potential evaporation during the growing season is between 1016 and 1270 mm [NOAA technical report NWS 33, 1982]. The region experienced very little precipitation during the duration of the study in the year 2004 [Bindlish et al., 2008]. The second region is in Iowa. The climate in the region is classified as “cold-without dry season-hot summer” (Köppen climate classification Dfa). The average annual rainfall in this region is 834.9 mm [Bindlish et al., 2006]. The potential evaporation during the growing season is 762 mm [NOAA technical report NWS 33, 1982]. During the period of study in 2002, no precipitation occurred for over 10 days before the soil moisture data collection began [Katzberg et al., 2006] after which locally heavy rainfall events were observed from day of year (DOY) 185–191. On DOY 192, there was a widespread rain event

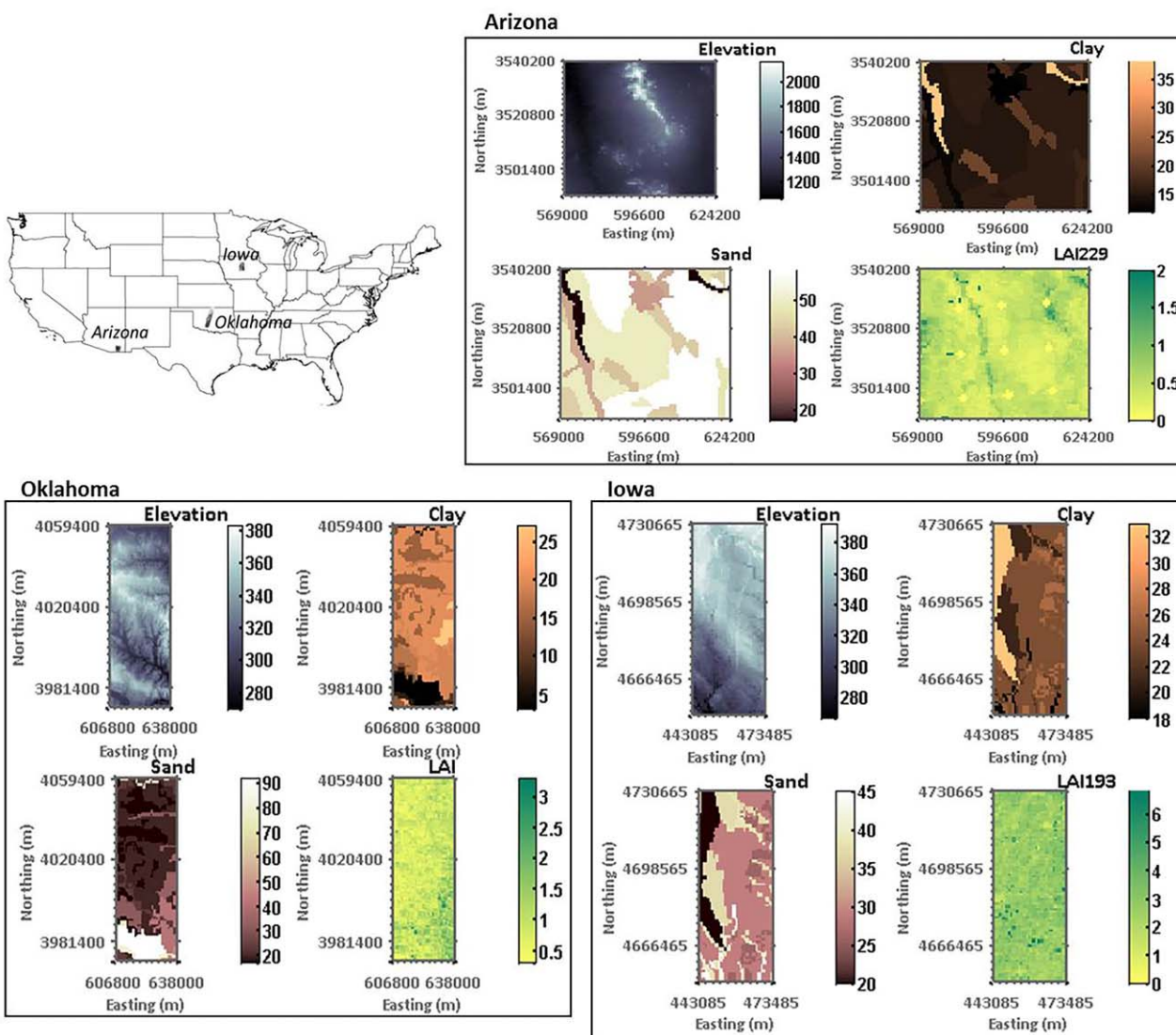


Figure 1. Site characteristics of the study sites.

[Jackson *et al.*, 2003]. The third study area is in Oklahoma and is characterized as “temperate-without dry season-hot summer” climate (Köppen climate classification Cfa). The average annual rainfall as recorded in the Little Washita watershed within the study region is ~749 mm [Jackson *et al.*, 1999]. The climate in the region remains humid throughout the year. The summers are hot and long while the winters are cool and short. Summer precipitation is dominated by convective precipitation. The potential evaporation during the growing season is between 914.4 and 1016 mm [NOAA technical report NWS 33, 1982]. During the period of study in 1997, three significant wetting events were observed in Oklahoma. Two events (DOY 176-177 and 180-181) had a strong north-south gradient with heavy precipitation in the northern half and little to no precipitation in the southern half. The third event (DOY 191-192) delivered nearly homogeneous rainfall to the entire study region [Crow and Wood 1999].

2.2. Data

The heterogeneity in topography, soil, and vegetation was described using various attributes for a comprehensive analysis. Topography was represented by elevation (DEM), slope, and flow accumulation, soil was represented by percent clay and percent sand, while leaf area index (LAI) was used to represent vegetation. The elevation data (30 m resolution) was obtained from the National Elevation Data set [Gesch *et al.*, 2009].

Table 1. Metrics of Properties Representing Different Physical Factors for Semiarid (Arizona), Humid (Iowa), and Subtropical (Oklahoma) Regions

Phys. Factor	Max	Min	Average	CV ^a	Median
Elevation (m)					
Arizona	2155.00	1074.00	1365.96	0.11	1335.00
Iowa	391.63	266.95	342.85	0.07	350.51
Oklahoma	383.00	269.99	328.32	0.06	327.67
Clay (%)					
Arizona	38.00	12.00	16.64	0.28	16.00
Iowa	33.00	18.00	24.76	0.14	24.00
Oklahoma	27.00	3.00	16.83	0.33	19.00
Sand (%)					
Arizona	58.00	17.00	50.00	0.19	49.00
Iowa	45.00	20.00	29.92	0.19	29.00
Oklahoma	92.00	17.00	31.51	0.72	20.00
Slope (m/m, [°])					
Arizona	0.310 [17.22°]	0.000 [0.03°]	0.028 [1.61°]	0.021 [1.22°]	0.018 [1.05°]
Iowa	0.023 [1.36°]	0.000 [0.00°]	0.004 [0.24°]	0.012 [0.66°]	0.004 [0.21°]
Oklahoma	0.027 [1.53°]	0.000 [0.01°]	0.006 [0.35°]	0.010 [0.59°]	0.005 [0.31°]
Flow Acc. ^b					
Arizona	1339.00	0.00	21.60	3.97	2.00
Iowa	129.00	0.00	4.37	2.58	0.00
Oklahoma	701.00	0.00	10.23	3.81	0.00
LAI ^c (m ² m ⁻²)					
Arizona	1.80	0.00	0.46	0.45	0.50
Iowa	6.80	0.10	2.62	0.33	2.50
Oklahoma ^c	3.3	0.3	0.96	2.68	0.9

^aCV represents coefficient of variation.

^bUnits are number of pixels (800 m × 800 m).

^cLAI data for Oklahoma were taken from the year 2004 since MODIS data were not available in 1997. Since Oklahoma is mostly natural grasslands which remain almost same across the years, data sets from different years with similar rainfall was considered.

The root mean square of the reported vertical accuracy of the data set is 1.55 m [Gesch *et al.*, 2014]. Slope (calculated in degrees) and flow accumulation were derived from the same elevation data set using ArcGIS (ESRI). Percent sand and clay values were obtained from Soil Geographic (STATSGO) Data Base for the Conterminous United States [Miller and White, 1998]. All available LAI data for the period of study were extracted from the 4 day composite MODIS product [NASA Land Processes Distributed Active Archive Center, 2001]. The algorithm to generate the composite LAI product chooses the “best” pixel from all the acquisitions of the MODIS sensors aboard NASA’s Terra and Aqua satellites from within a 4 day period. The three study regions vary extensively in terms of soil, vegetation, and topography. Arizona has the highest sand content on average with very little vegetation which is mostly in the form of shrubs with some pasture and cropland. The topography includes areas of high relief with a generally undulating terrain. Iowa has fertile soils with corn and soybean comprising the dominant vegetation in the entire domain. The terrain varies smoothly across the domain. Oklahoma has the widest range of sand and clay content amongst the three regions. Vegetation comprises mostly of pasture with some cropland while the terrain is gently rolling. Statistics describing site characteristics have been given in Table 1.

Airborne volumetric soil moisture data (Figures 2a and 2b) for Iowa and Arizona were collected during Soil Moisture Experiments in 2002 (SMEX02) and 2004 (SMEX04) respectively, using the Polarimetric Scanning Radiometer, PSR [Bindlish *et al.*, 2006, 2008] at 800 m × 800 m spatial resolution. The data for Oklahoma (Figure 2c) was collected in 1997 (Southern Great Plains (SGP) 1997 hydrology experiment) using the Electronically Scanning Radiometer [Jackson *et al.*, 1999] at 800 m × 800 m spatial resolution. The soil moisture data comprise a wide range of soil moisture conditions (Figure 2) that are representative of the typical soil moisture conditions in the regions during the growing season. The airborne soil moisture data were validated against the corresponding field averages of the ground-based soil moisture data that was collected simultaneously. The standard errors of the airborne data as compared to ground-based data were small—0.014 cm³/cm³ (v/v) for Arizona [Bindlish *et al.*, 2008], 0.055 cm³/cm³ for Iowa [Bindlish *et al.*, 2006], and ~0.03 cm³/cm³ for Oklahoma [Jackson *et al.*, 1999]. Thus, the moisture retrieval algorithm used was assumed to not bias the interpretation of the results in this study.

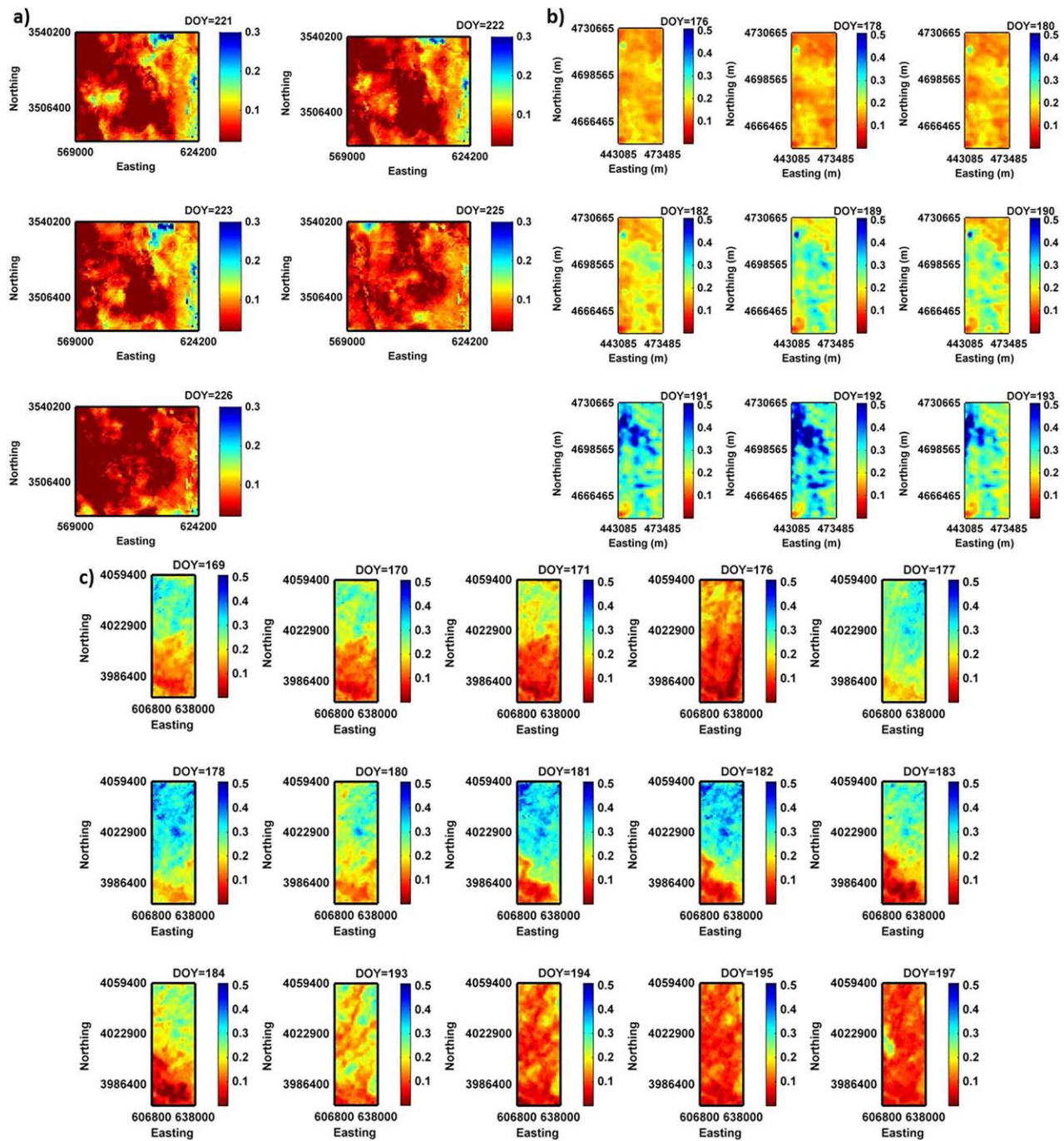


Figure 2. Volumetric soil moisture maps for (a) Arizona, (b) Iowa, and (c) Oklahoma regions.

3. Methodology

Land-surface based physical factors (also referred to as biophysical factors or biophysical controls in the study) mainly affect soil moisture dynamics by redistributing/changing the available moisture content in the land surface. Soil moisture changes as opposed to absolute values of soil moisture have been shown to be more related to landscape factors [Logsdon, 2015] and also more accurate [Green and Erskine, 2011]. Moisture redistribution or changes in soil moisture content in a region over a given period of time, takes place as a result of infiltration/drainage (primarily dependent on soil type) or evapotranspiration (dependent on vegetation, soil, and topography) from within a pixel and also subsurface/overland flow (dependent

Table 2. Days of Year (DOY) Data Were Available for and the Time and Spatial Scales at Which the Wetting/Drying Dynamics Were Analyzed

Region	Data Availability (DOY)	Time Scales Analyzed (days)	Spatial Support Scale (km)	Data Dimension (pixels)
Arizona	221–223,225–226	1–2	1.6, 3.2, 6.4, 12.8	4340 (62 × 70)
Iowa	176,178,180,182,185,189–193	1–2	1.6, 3.2, 6.4, 12.8	3900 (100 × 39)
Oklahoma	169–171,176–178,180–184,193–195,197	1–2	1.6, 3.2, 6.4, 12.8	4440 (111 × 40)

on soil and topography) between pixels etc. Since each process causing redistribution has its own associated time scale, a redistributed soil moisture signal sampled over different time scales may reveal a dominance of different physical processes. Thus, moisture redistribution at a fixed time scale (representative of RS data) was selected as the variable for evaluating controls of biophysical factors on footprint scale soil moisture dynamics. The magnitude of soil moisture redistribution is also a function of antecedent moisture conditions and depends on whether the domain is undergoing drying or wetting as evident by hysteresis observed in past studies [Teuling *et al.*, 2007; Ivanov *et al.*, 2010; Gaur and Mohanty, 2013]. Thus, in order to study the effect of land-surface factors on soil moisture dynamics in isolation, the effect of antecedent soil moisture from the moisture redistribution spatial signal was removed. Since the functional dependence of moisture redistribution on biophysical factors also changes with seasons which act as a large temporal scale forcing, the results from this study are representative only of the growing season.

We generated pixel-based daily (in some cases, once in 2 days or bidiurnal) moisture redistribution images. The daily (and bidiurnal) scale was selected keeping in mind that most satellite-based soil moisture data are typically available once every day. The influence of biophysical factors on moisture redistribution was computed in terms of their areal extent of dominance and the average magnitude of moisture redistribution they cause. The areal extent was evaluated by comparing the spatial patterns of the redistribution signal with the patterns of different land-surface based biophysical factors. It was assumed that if a biophysical factor contributed to moisture redistribution, the spatial pattern of moisture redistribution would reflect the spatial pattern of the same biophysical factor. For example, the spatial patterns of vegetation would match that of moisture redistribution if evapotranspiration was the dominant process causing redistribution. The results were analyzed for drying and wetting conditions separately to account for any large-scale hysteresis. The computational details of the methodology are given below.

Using the soil moisture data for each region, soil moisture redistribution (equations (1) and (2)) values were computed. Soil moisture data were collected at irregular time intervals. Thus, the redistribution values represent soil moisture redistribution over time scales ranging from 1 to 2 days depending on the duration between two consecutive airborne remote sensing data collection days (Table 2).

$$\Delta SM_t = sm_t - sm_{t-1(t-2)} \quad (1)$$

ΔSM_t = redistributed soil moisture for day, t (before correction for antecedent soil moisture, $sm_{t-1(t-2)}$)

sm_t = soil moisture for day, t

Figure 3 shows a monotonic decreasing relationship between antecedent soil moisture and moisture redistribution. Thus, in order to evaluate the significance of different biophysical factors on moisture redistribution in isolation from the effect of antecedent moisture, the redistribution values were normalized using antecedent moisture values for each pixel (equation (2))

$$\Delta SM_{norm,t} = \frac{\Delta SM_t}{SM_{ant}} \quad (2)$$

$\Delta SM_{norm,t}$ = soil moisture redistribution at a pixel after correction for antecedent moisture

SM_{ant} = antecedent soil moisture at the pixel, $sm_{t-1(t-2)}$

Note that the soil moisture redistribution was not normalized with respect to duration of redistribution (1 or 2 days) since it would imply that half of the redistribution took place on the first day while the other half on the second day. Our current knowledge of soil moisture dynamics at larger scale which may only be considered to be an approximation of the Richard's equation, developed for local scale soil water flow behavior

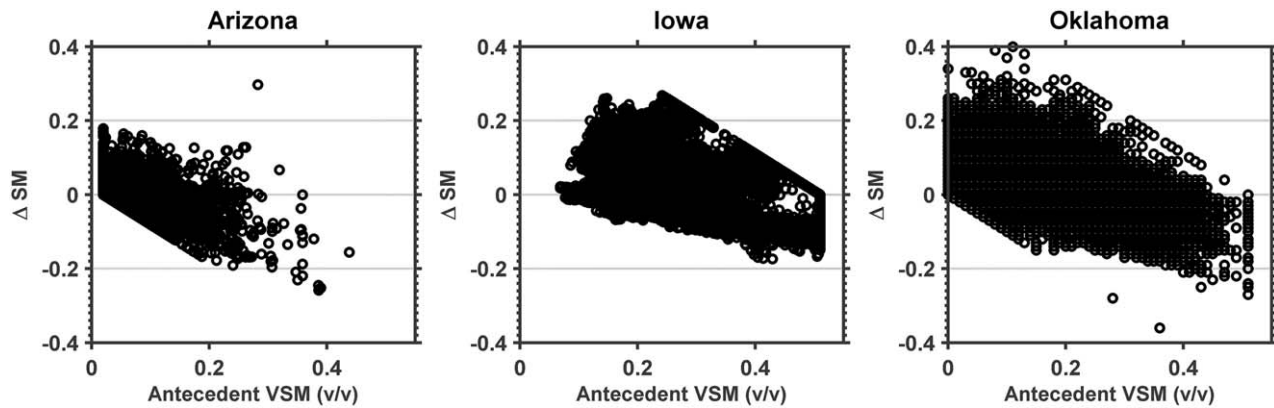


Figure 3. Plot of observed ΔSM given antecedent volumetric soil moisture conditions.

indicates that soil moisture dynamics are nonlinear. A linear rate of change (such as dividing by number of days) may misrepresent the soil moisture dynamics.

The factors representing soil (original resolution 1000 m), vegetation (original resolution 1000 m), and topography (original resolution 30 m) were resampled (using the nearest neighbor method) to 800 m in order to maintain consistency in the data resolution of the biophysical factors and soil moisture. The nearest neighbor interpolation scheme is typically considered best in case of discrete raster data sets. Slope and flow accumulation were computed from the resampled elevation data sets. A study [Wu et al., 2008] on effect of resampling methods of elevation data in Southwest Virginia also showed minor differences in computed slopes as a result of resampled elevation data using different resampling techniques.

3.1. Wavelet Analysis

In order to extract support-scale-based information from the images comprised of the moisture redistribution values as well as the biophysical factors, two-dimensional nondecimated wavelet (NDWT) analysis was used. Wavelet analysis has proven to be a powerful tool in understanding geophysical data [Kumar and Foufoula-Georgiou, 1997; Si and Zeleke, 2005] in both temporal and spatial domains [e.g., Kumar and Foufoula-Georgiou, 1993; Strand et al., 2006]. Wavelets are “wave like” functions, $\psi(x)$, defined at a location “ x ” which oscillate about the x axis and satisfy three criteria (1) $\int_{-\infty}^{\infty} \psi(x) dx = 0$, i.e., zero mean value, (2) $\int_{-\infty}^{\infty} |\psi(x)|^2 dx = 1$, i.e., finite energy, and (3) compact support, i.e., nonzero value over a narrow interval. Once a particular formulation of the “mother wavelet” (or basis function), $\psi(x)$, is fixed, it is scaled (dilated) and translated over a given signal (equation (3)) and the resultant variations serve as basis functions ($\psi_{s,u}(x)$) to represent the given signal.

$$\psi_{s,u}(x) = \frac{1}{\sqrt{s}} \psi\left(\frac{x-u}{s}\right) \quad (3)$$

s = scaling parameter which controls the dilation

u = location of wavelet used for translation across the signal

NDWT is a discrete wavelet transform. For a discrete wavelet transform (DWT), any discrete signal X_n ; $n = 0, 1, \dots, N-1$ is decomposed into wavelet coefficients, $W_{s,u}$ for each scale (s) and location (u), through wavelets. Simply explained a wavelet coefficient, $W_{s,u}$, represents the degree of similarity between the wavelet at the scale “ s ” and at location determined by “ u ” and the signal at the same location. The higher the wavelet coefficient, greater is the similarity. The set of all wavelet coefficients “ \tilde{W}_s ” for scale, “ s ” can be described as given in equation (4).

$$\tilde{W}_s = \sum_{u=0}^{2s-1} \psi_{s,u}(x) \cdot X_{n-u} \quad (4)$$

The basis functions in the case of a DWT scale up in a dyadic series represented by equation (5). The largest scale of the basis function is restricted by the length of the data set (less than half the dimension of the data).

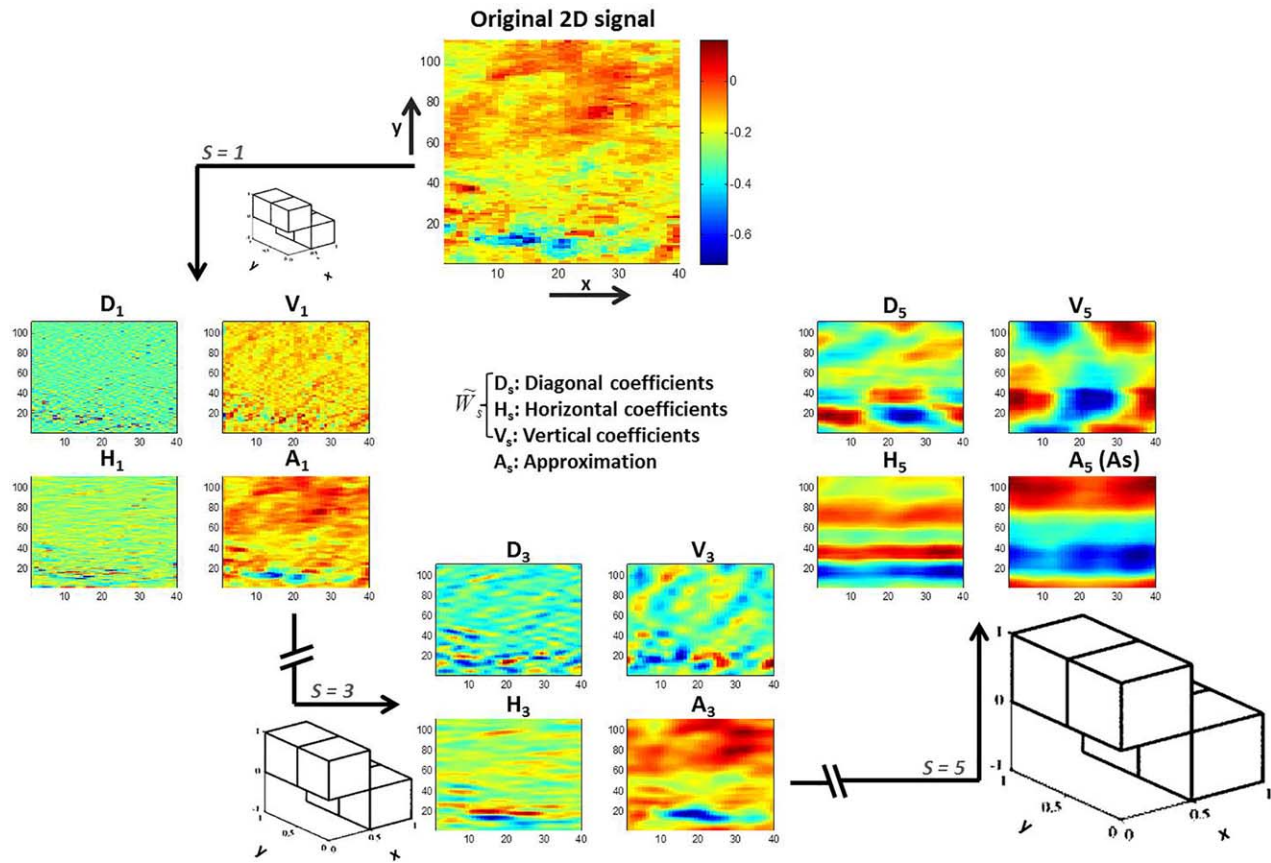


Figure 4. Diagrammatic representation of nondecimated wavelet analysis. A dilated (scaled) HAAR wavelet is run on each subsequent approximation of the previous scale to obtain (H,V,D details). Some scales have been omitted for brevity.

$$\psi_{s,u}(x) = 2^s \psi(2^s x - u); \quad s = 1, 2, \dots \quad (5)$$

The mother wavelet chosen for our study was the Haar wavelet represented by equation (6). Soil moisture spatial signals commonly display rapid changes as may be observed after localized rainfall events. A Haar wavelet was chosen given its suitability in detecting rapid changes [Mahrt, 1991]. The Haar wavelet has also been recommended for soil moisture applications in literature [Das and Mohanty, 2008].

$$\psi_{s,u}(x) = \begin{cases} 1 & 0 \leq x < 0.5 \\ -1 & 0.5 \leq x < 1 \\ 0 & \text{otherwise} \end{cases} \quad (6)$$

We performed a two-dimensional NDWT on our spatial data. A 2-D wavelet transform is a wavelet transform performed twice—once on the rows and once on the columns of the image. It produces horizontal, vertical, and diagonal details and an approximation (Figure 4) for scale ranges represented by “s”. The approximation represents the original signal after the details at support scale range, “s”, have been removed from the signal. While running wavelet analysis, each wavelet transform is conducted on the approximation of the next finer-scale range (Figure 4). Thus, after running the wavelet analysis over all possible scales, the result is a set of details at all scales “S” and a signal approximation (A_S). A_S represents the large-scale residual after information of the finer support scales has been extracted through detail wavelet coefficients. The horizontal details are obtained by passing high pass-low pass (HP-LP) filters, vertical details by passing LP-HP and diagonal details are obtained by passing HP-HP filters over the domain over each normalized soil moisture redistribution and biophysical factors’ image separately. The hyphenated combination indicates the vertical-horizontal direction in which filters are moved. The set of all wavelet coefficients (\tilde{W}_s) at a particular scale range, s, represents the “details” in the signal at that particular scale.

NDWT is associated with zero phase filter and is translation invariant. It thus results in images of the wavelet coefficients which can be perfectly aligned with the original signal [Percival and Walden, 2000] and reduces error in interpretation resulting from the sampling scheme/starting point of the data. For more mathematical details on NDWT, the readers are referred to Percival and Walden [2000]. The NDWT wavelet analysis on our data set was carried out using the waveslim package [Whitcher, 2012] in the statistical software package R version 3.0.1, R core team [2013].

Wavelets analysis (like Fourier analysis) is computed in the frequency domain of the (in this case, spatial) signal and provides information of the range of support scales corresponding to different frequency bands. In the given study, the data set was analyzed over four support scale ranges (1.6–3.2 km, 3.2–6.4 km, 6.4–12.8 km, 12.8–25.6 km) that represent corresponding ranges of spatial frequency. The scale ranges have been referred to by their lower scale limit in the results and discussion.

A useful property of NDWT is that it divides the total variance of the signal, $\sigma^2(X_n)$ into the components of variance associated with different support scales. The total variance of the signal can be reconstructed by simple addition [Percival et al., 2011] as explained in equation (7).

$$\sigma^2(X_n) = \sum_{s=1}^S \sigma^2(\tilde{W}_s) + \sigma^2(A_s) \quad (7)$$

$\sigma^2(X_n)$ is defined as the statistical variance = $\sum \frac{(X-\bar{X})^2}{n-1}$, where X is the normalized moisture redistribution variable, \bar{X} is the sample mean and n is number of realizations of the variable. $\sigma^2(\tilde{W}_s)$ or the global wavelet spectrum is the variance contributed by support scale range, s , to the variance of the signal, $\sigma^2(X_n)$ which can also be obtained by adding the variance of the detail wavelet coefficients (horizontal, vertical, and diagonal) of an image at each support scale range. Thus, wavelets can characterize a nonstationary spatial/temporal data set at different support scales (coarser than the scale of the original signal).

In the given study, the global wavelet spectrum was modified (equation (8)) to understand the percentage of variance ($\sigma_{global}^2(\%)$) contributed by a particular support scale range to the total variance of moisture redistribution signal.

$$\sigma_{global}^2(\%) = \frac{\sigma^2(\tilde{W}_s)}{\sigma^2(X_n)} \times 100 \quad (8)$$

3.2. Pattern Matching

The contribution of different biophysical factors to soil moisture redistribution was computed in terms of its areal extent of influence and the magnitude of moisture redistribution associated with the physical factor. The spatial patterns of the biophysical factor were matched with the patterns of the moisture redistribution signal at different support scales. The areal extent of impact was determined by calculating the total area at which pattern matches between the biophysical factor and $\Delta SM_{norm,t}$ were observed. A successful match in the pattern of $\Delta SM_{norm,t}$ and the biophysical factor was computed by equating the wavelet spectrum (*individually squared wavelet coefficient, $W_{s,norm}^2$ (defined below)*) of the two signals for each spatial support scale. The wavelet spectrum was computed using the horizontal, diagonal, and vertical details of each $\Delta SM_{norm,t}$ and biophysical factor image. Location-specific wavelet spectrum values that differed by less than 0.005, were considered to display a similar pattern at the particular location and scale. The threshold value of 0.005 was decided subjectively so that the matching criteria could be strict (close to 0) while allowing some scope of uncertainty in the measured soil moisture and biophysical factors' data. Prior to comparison of the wavelet spectrum of the physical factors and $\Delta SM_{norm,t}$, the wavelet coefficients for each individual $\Delta SM_{norm,t}$ and biophysical factors' image were separately normalized (equation (9)) with mean of 0 and standard deviation of 1. The mean and standard deviation for normalizing the coefficients were calculated after removing the outliers. It was necessary to remove outliers to clean the data set of water bodies, normalized soil moisture redistribution computed where antecedent soil moisture was set to 0 and unrealistic flow accumulation values because of edge effects. The outliers were determined and removed using equation (10).

$$W_{s,norm} = \frac{W_{s,k} - \frac{1}{K} \sum_{k=1}^K W_{s,k}}{\sqrt{\frac{1}{K} \sum_{k=1}^K \left(W_{s,k} - \frac{1}{K} \sum_{k=1}^K W_{s,k} \right)^2}} \quad (9)$$

where $k = 1, 2, \dots, K$ = number of pixels in the domain

$$W_{s,outlier} : \begin{aligned} & W_s > \frac{1}{K} \sum_{k=1}^K W_{s,k} + 2 \sqrt{\frac{1}{K} \sum_{k=1}^K \left(W_{s,k} - \frac{1}{K} \sum_{k=1}^K W_{s,k} \right)^2} \\ & W_s < \frac{1}{K} \sum_{k=1}^K W_{s,k} - 2 \sqrt{\frac{1}{K} \sum_{k=1}^K \left(W_{s,k} - \frac{1}{K} \sum_{k=1}^K W_{s,k} \right)^2} \end{aligned} \quad (10)$$

Equation (11) was then used to determine the relative areal extent of influence of the biophysical factors (e.g., soil, topography, and vegetation) on $\Delta SM_{norm,t}$ at different support scale ranges.

$$C_{f,s} = \frac{N_{f,s}}{N_{\sum f,s}} \times 100 \quad (11)$$

$C_{f,s}$ = percent contribution of biophysical factor, f at a specific support scale range, s

$N_{f,s}$ = number of pattern matches of a specific biophysical factor, f , at a specific support scalerange, s

$N_{\sum f,s}$ = total number of pattern matches observed for all biophysical factors at a particular support scale range, s .

The magnitude of controls ($M_{f,s}$) of each biophysical factor, f , at scale, s , was computed by evaluating the mean of $\Delta SM_{norm,t}$ for the pixels where a pattern match between the biophysical factor, f and $\Delta SM_{norm,t}$ was observed (equation (12)).

$$M_{f,s} = \frac{1}{N_{f,s}} \sum_{N_{f,s}} \Delta SM_{norm,t} \quad (12)$$

$C_{f,s}$ and $M_{f,s}$ were computed separately for drying (negative values of ΔSM_t) and wetting (positive values of ΔSM_t) scenarios to account for any hysteretic behavior of the region.

4. Results and Discussion

Normalized soil moisture redistribution, $\Delta SM_{norm,t}$ was computed over 1 or 2 day intervals. The 2 day interval soil moisture redistribution values were calculated when the soil moisture data were not collected daily because of rain events or logistic reasons. Table 2 provides the details of available data for each study region. The $\Delta SM_{norm,t}$ computed for day of year (DOY) 225 (in Arizona), DOY 178, 180, and 182 (in Iowa) and DOY 180, and 197 (in Oklahoma) represent soil moisture redistribution computed over 2 day periods.

4.1. Analysis of Variance of $\Delta SM_{norm,t}$

The variance of a soil moisture signal is dependent on the support scale it is sampled at [Blöschl and Sivapalan, 1995]. The total variance of the original $\Delta SM_{norm,t}$ signal represents the variance in soil moisture dynamics at the 0.8 km support scale which contains information of scales at and coarser than 0.8 km (restricted by extent of data). The variance within the 0.8 km support scale has been averaged within the data set and cannot be represented by this data. The NDWT based analysis divides the variance of the original spatial signal (0.8 km support scale) into variance contributed by different spatial support scale ranges i.e., 1.6-3.2, 3.2-6.4, 6.4-12.8, and 12.8-25.6 km. Figure 5 shows the percent contribution ($\sigma_{global}^2(\%)$ (8)) of each support scale to the total variance of spatial $\Delta SM_{norm,t}$ signal. Increasing trends indicate that even data collected at coarse remote sensing resolutions can account for most of the soil moisture dynamics within a region whereas a decreasing trend indicates that coarse resolution data set will be insufficient to account for the soil moisture dynamics. The daily variance signals showed typical increasing trend up to 6.4 km spatial resolution for all days in Iowa and a few days in Arizona and Oklahoma (Figure 5). However, the lack of a consistent trend in the global wavelet spectrum indicates that the contribution of different spatial support scales to soil

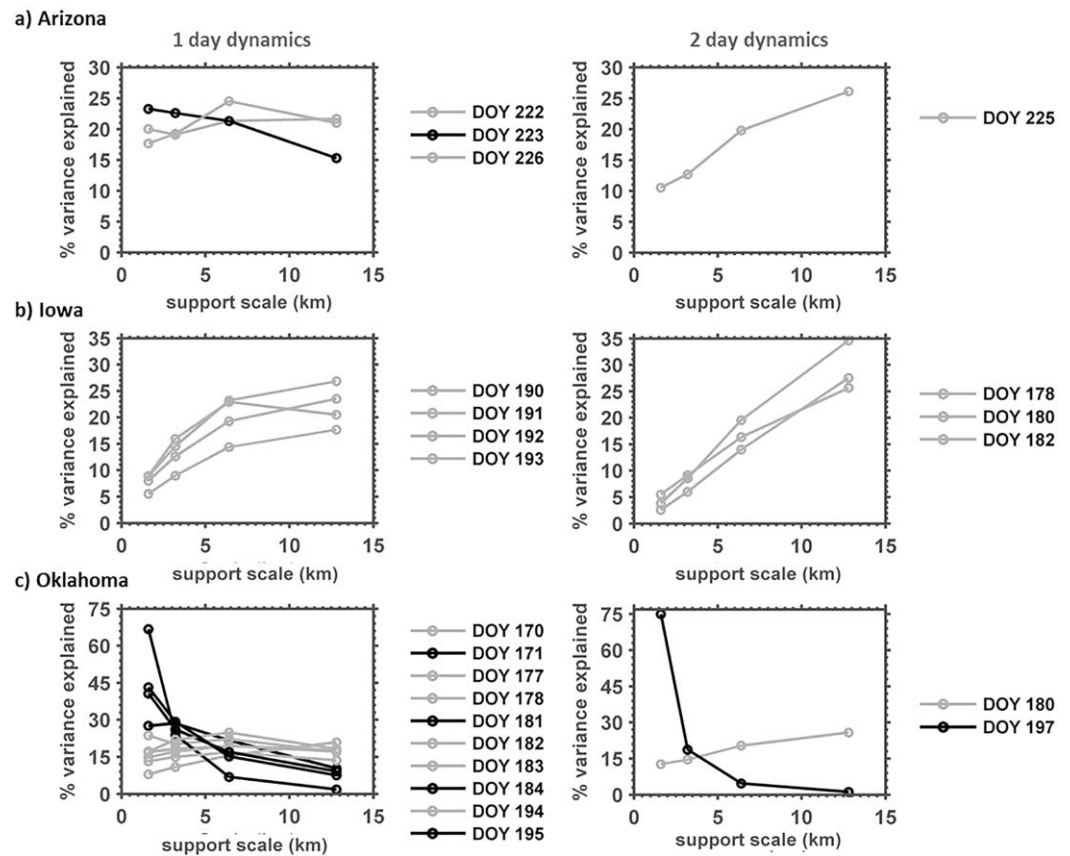


Figure 5. Graphs depict percent of the total variance (equation (8)) observed in the soil moisture change signal at different scales for (a) Arizona, (b) Iowa, and (c) Oklahoma. 1 day and 2 day dynamics represent soil moisture change observed at 1 day and 2 days' interval, respectively.

moisture dynamics is not constant across time and varies at daily temporal scales within the growing season. This varied behavior is potentially caused by a combination of the antecedent moisture conditions, the land-surface heterogeneity, and meteorological forcings which vary dynamically in time. However, it is beyond the scope of this paper to investigate those combinations.

4.2. Scale-Based Contribution of Biophysical Factors

The scale-based contribution of the biophysical factors to soil moisture redistribution was evaluated as a function of their areal extent (equation (11)) of influence and the relative magnitude of their effect (equation (12)) on soil moisture redistribution. The analysis was conducted separately for drying and wetting conditions to account for large-scale hysteresis.

4.2.1. Areal Extent of Controls, $C_{f,s}$

The patterns observed in different physical factors and $\Delta SM_{norm,t}$ signals were matched (as described in section 3.2) for the three study regions. A sample diagrammatic representation of locations of pattern match between moisture redistribution patterns and % sand values is shown in Figure 6. Figures 6a and b depict the normalized wavelet coefficients of $\Delta SM_{norm,170}$ (Oklahoma) and % sand respectively while Figure 6c depicts the locations of the pixels where a pattern match between the two was observed. The white pixels correspond to the central location of the wavelet at which a pattern match was observed. Note that they do not represent the actual area (much larger) of the domain that we observe a pattern match for. The percentage of area of the domain that the white pixels comprise of is shown in Figure 7. A comparison of the three regions shows that Iowa distinctly has lesser areas of pattern matches between any physical factor and soil moisture redistribution at all scales as compared to Oklahoma and Arizona. The number of pattern matches of moisture redistribution with soil and topography in Arizona are higher than that of Oklahoma which has

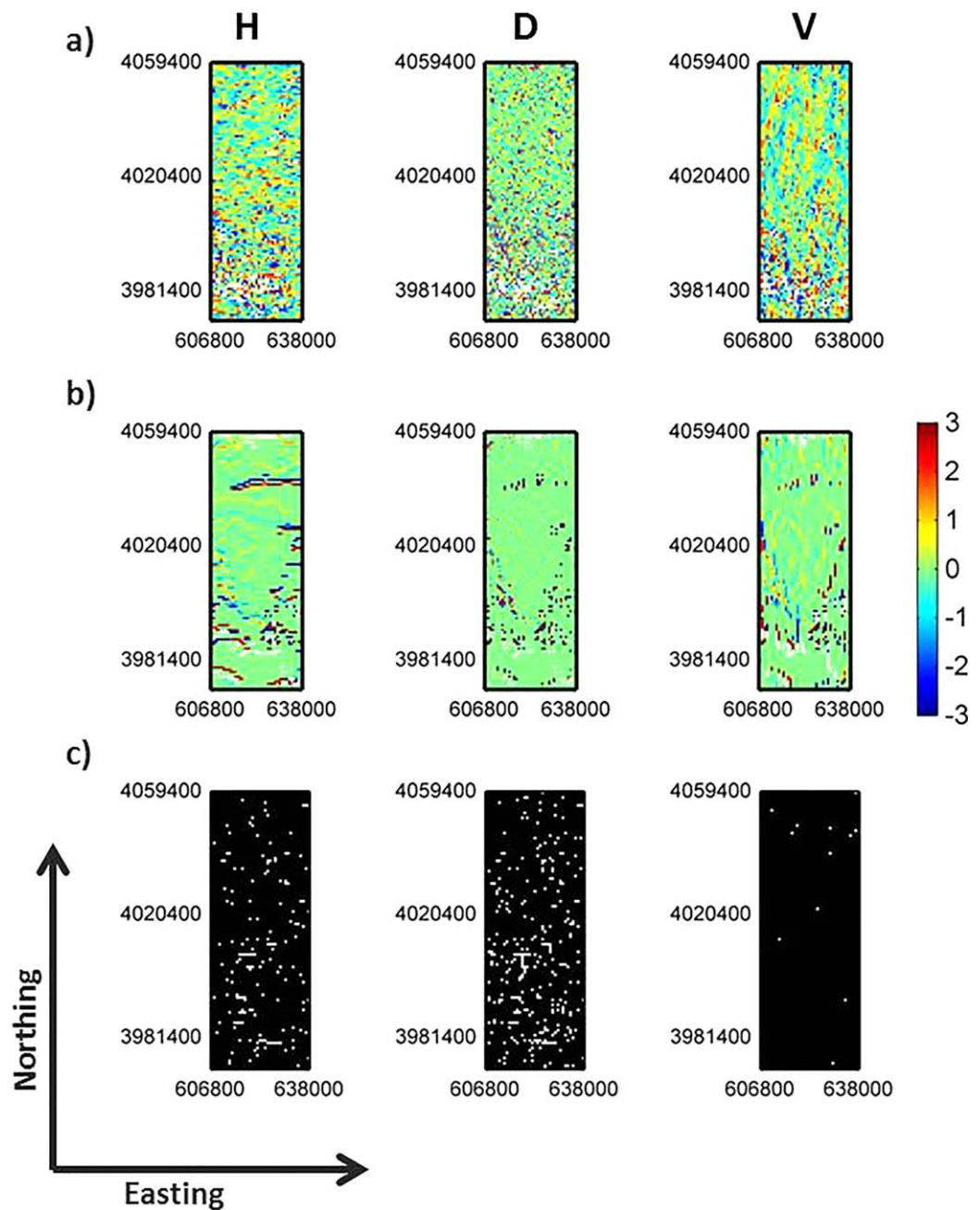


Figure 6. (a) Normalized wavelet coefficients for soil moisture redistribution (DOY 170), (b) Normalized wavelet coefficients for % sand, (c) Locations of pattern match (white pixels), in Oklahoma at 1.6–3.2 km scale.

the highest pattern matches with vegetation. The contribution of soil in the drying pixels in Arizona is significantly higher (~30%) than in the wetting pixels (~8%) at the 1.6 km scale and the trend is similar at the other scales. The number of pattern matches of all land-surface based physical factors with soil moisture redistribution decreases with increasing spatial support scales for all regions except for vegetation in Oklahoma which remains approximately similar.

The contribution of different physical factors relative to each other (equation (11)) is shown in Figure 8. The contribution of soil (% sand and % clay) remains high in all three hydroclimatic regions while maintaining a decreasing trend as we go higher in scale. The trend for contribution of topographical and vegetation factors, on the other hand, increases with increasing scale. Specifically, in Arizona, at 12.8 km, the effect of

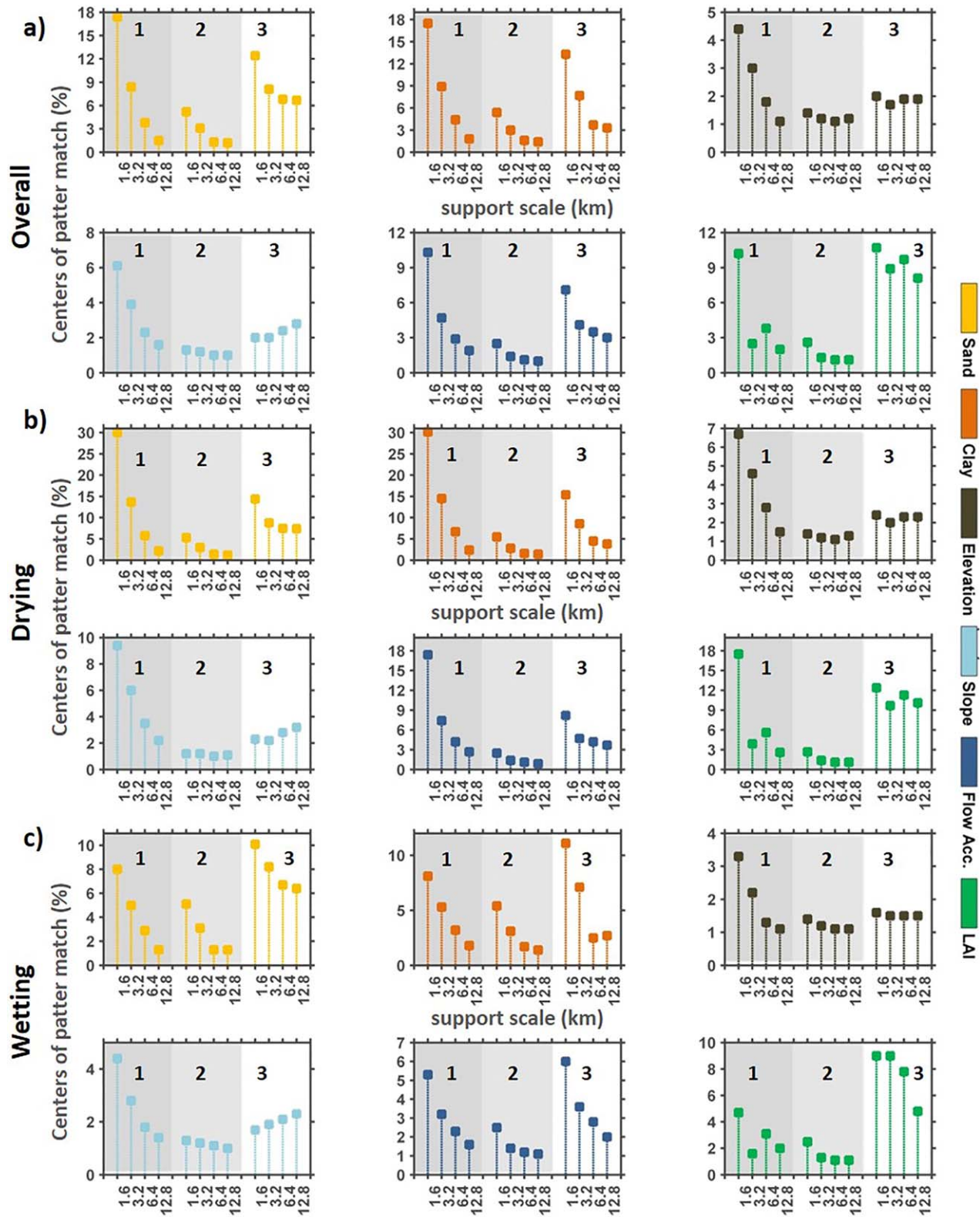


Figure 7. Percentage of white pixels (centers of wavelets for pattern match) for (1) Arizona, (2) Iowa, and (3) Oklahoma for different physical factors.

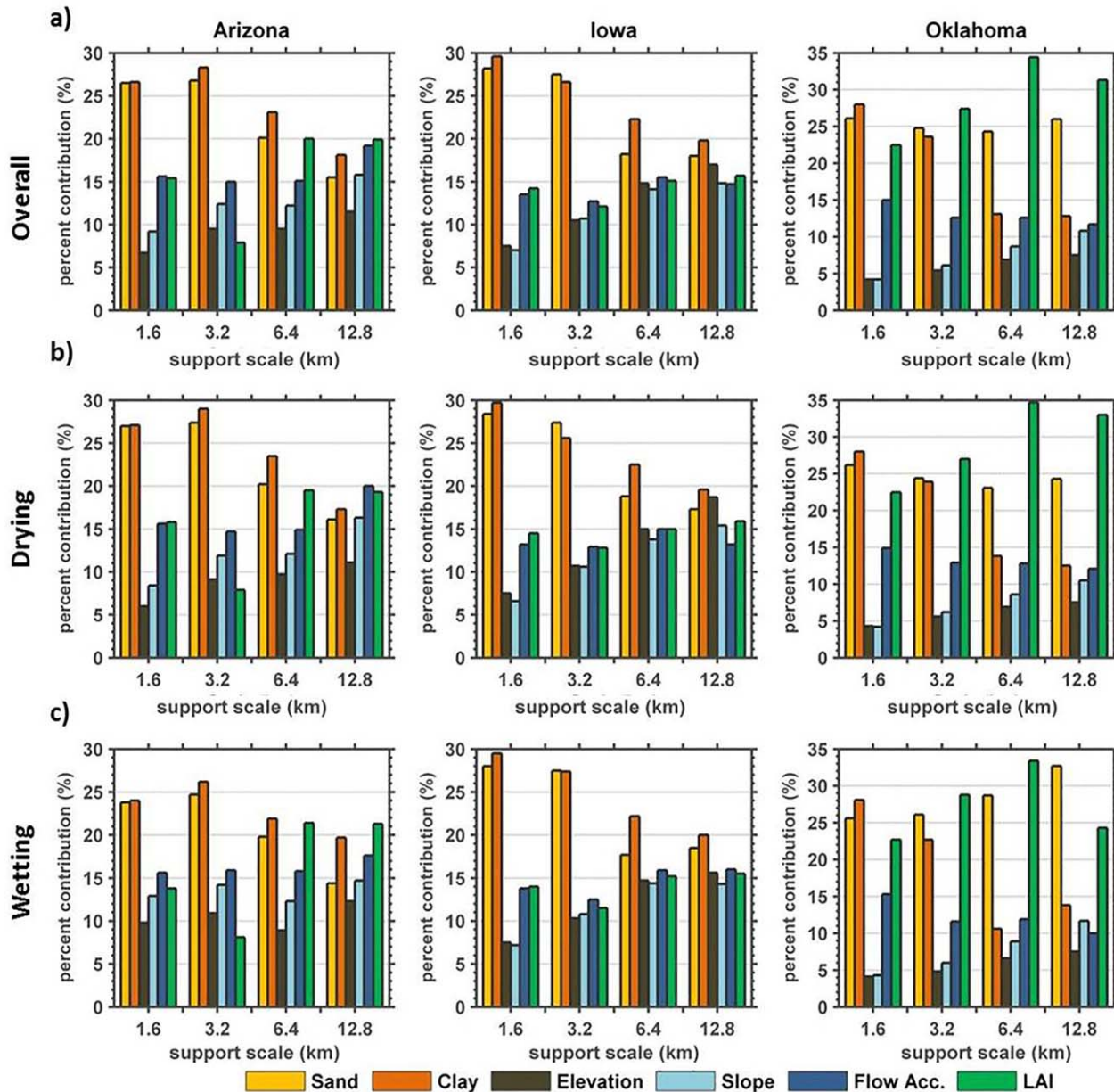


Figure 8. Percent contribution of different physical controls to soil moisture redistribution observed in Arizona, Iowa, and Oklahoma, (a) all pixels, (b) drying pixels, and (c) wetting pixels.

topography and vegetation becomes equivalent or slightly greater than soil. Also in Oklahoma, vegetation becomes more dominant than soil beyond 3.2 km. These factors are analyzed in greater detail below.

4.2.1.1. Soil Factors

Percent clay and sand: the percentage of clay and sand together define the infiltration capacity and water holding capacity of the domain at the land surface. Since they comprise the primary factors determining the pore sizes and structure of the soil in which water is being held, they also affect the rate of evaporation from the soil. Significant association between soil based factors and soil moisture change is evident in all three regions. Higher clay content can be related to higher water holding capacity of the soil. It also slows down infiltration and hinders drainage. The clay content can also cause the soil to aggregate and become fractured which would promote drainage under very wet conditions. However, the soils in our study regions are not fractured. In contrast, sand promotes increased infiltration. The spatial distribution of sand and clay across the study scales also determine infiltration versus evaporation patterns [Nachshon et al., 2011; Zhu and Mohanty, 2002a, 2002b; Mohanty and Zhu, 2007].

The contribution of % clay on soil moisture variability is higher than that of % sand in Arizona and in Iowa (except for the 3.2 km scale), whereas in Oklahoma % sand contributes more than % clay (except for the 1.6 km scale). This is true for drying as well as wetting scenarios. Arizona is semiarid and usually remains relatively dry. Under these conditions, any moisture that is held in the soils is held by the small pores represented by % clay as opposed to % sand. The greater pattern association with % clay in Arizona represents that the evaporation is the dominant process of water redistribution as opposed to drainage of free water [Zhu and Mohanty, 2002a, 2002b]. Despite being a sandy region, the water dynamics in Arizona are controlled (limited) by the clay content in the soil. In case of Iowa, which is primarily a cultivated region that receives higher precipitation than semiarid Arizona, soil moisture patterns match well with both % sand and % clay. This indicates that both processes (evaporation and drainage) occur in this region to cause redistribution of moisture. Iowa is a cropped land planted with soybean and corn. The canopies of the two crops (during initial period of growth) allow bare soil exposure to the sun. Thus, the top soil made porous by plant roots enables infiltration (represented/limited by % sand) whereas the landcover promotes water losses (represented/limited by percent clay) through evapotranspiration. Oklahoma is a subhumid region and the major losses to the near-surface soil moisture are due to drainage represented/limited by % sand. Thus, the influence of soil texture on soil moisture redistribution is directly linked to the hydroclimate and wetness condition of a region.

4.2.1.2. Topographic Factors

Elevation, slope, and flow accumulation: elevation is the basic topographic factor from which a number of heterogeneity representing parameters (slope, flow accumulation etc.) may be derived. Elevation patterns can relate to soil moisture patterns for different reasons [Coleman and Niemann, 2013]. It may cause steep potential gradients thus, influencing moisture redistribution. Large elevation differences induce differences in evapotranspiration (because of vegetation gradients) and changing precipitation patterns with elevation [Goulden et al., 2012]. Slope can strongly influence water distribution through overland flow or aspect-based drying. Flow accumulation represents the tendency of the region to accumulate water (concavity) and thus, the water holding capacity of a region. This may lead to localized infiltration and evaporation.

Figure 8a shows that the behavior of topography (elevation, slope, and flow accumulation) with scale is similar for all three hydroclimates, i.e., its percent contribution increases with support scale. In the relatively natural (anthropogenically unaltered) and topographically more complex (undulating terrain) regions, Oklahoma and Arizona, flow accumulation has a higher contribution than slope and elevation, whereas the trend is different for Iowa where elevation takes a higher precedence at coarser scales (6.4 km and coarser).

Overall, we observe that Arizona and Oklahoma behave similarly whereas the behavior of moisture dynamics in Iowa is different. Oklahoma and Arizona are topographically more complex than Iowa which has a relatively smoothly varying north to south gradient (Figure 1). Even though the absolute values of elevations in Iowa and Oklahoma are similar, the pattern association for the two regions is very different. This implies that the spatial patterns of elevation (or some derivative of elevation) dictate the effect of elevation on soil moisture redistribution. Oklahoma is rolling and thus, the concavity of the domain remains an important factor whereas the slope in Iowa is more uniform and therefore the effect of concavity of the domain becomes lesser than elevation as we go higher in scale. The contribution of slope is mostly slightly higher for the wetting pixels than drying pixels in Oklahoma and Arizona (Figures 8b and 8c). The contribution of elevation is only marginally different during wetting and drying. The higher contribution of slope in the two regions during wetting signifies the occurrence of overland flow in Oklahoma and even in the precipitation limited Arizona. However, in Iowa, the trend is different with elevation showing higher contribution for the drying pixels. The contribution of elevation in Iowa also becomes equivalent comparable to or larger than other topographical factors at the coarser scales (6.4 km and coarser). This signifies two important points. First, elevation influences drying more than wetting in these regions. This could be because of higher influence of elevation on evapotranspiration patterns than precipitation in these regions. Second, irrespective of the precipitation dynamics, in topographically less undulating regions, the contribution of topography on soil moisture spatial distribution is more dominated by the elevation of a pixel. On the other hand in topographically complex (undulating) regions, flow accumulation and slope form better representative parameters of topography for describing soil moisture spatial dynamics.

4.2.1.3. Vegetation Factors

Leaf area index: leaf area index is a proxy for vegetation. It can cause soil moisture loss through transpiration, restrict evaporation from the ground surface by shading the ground surface and limit the amount of input water through interception and evaporation of intercepted water on the leaf. It can also direct water

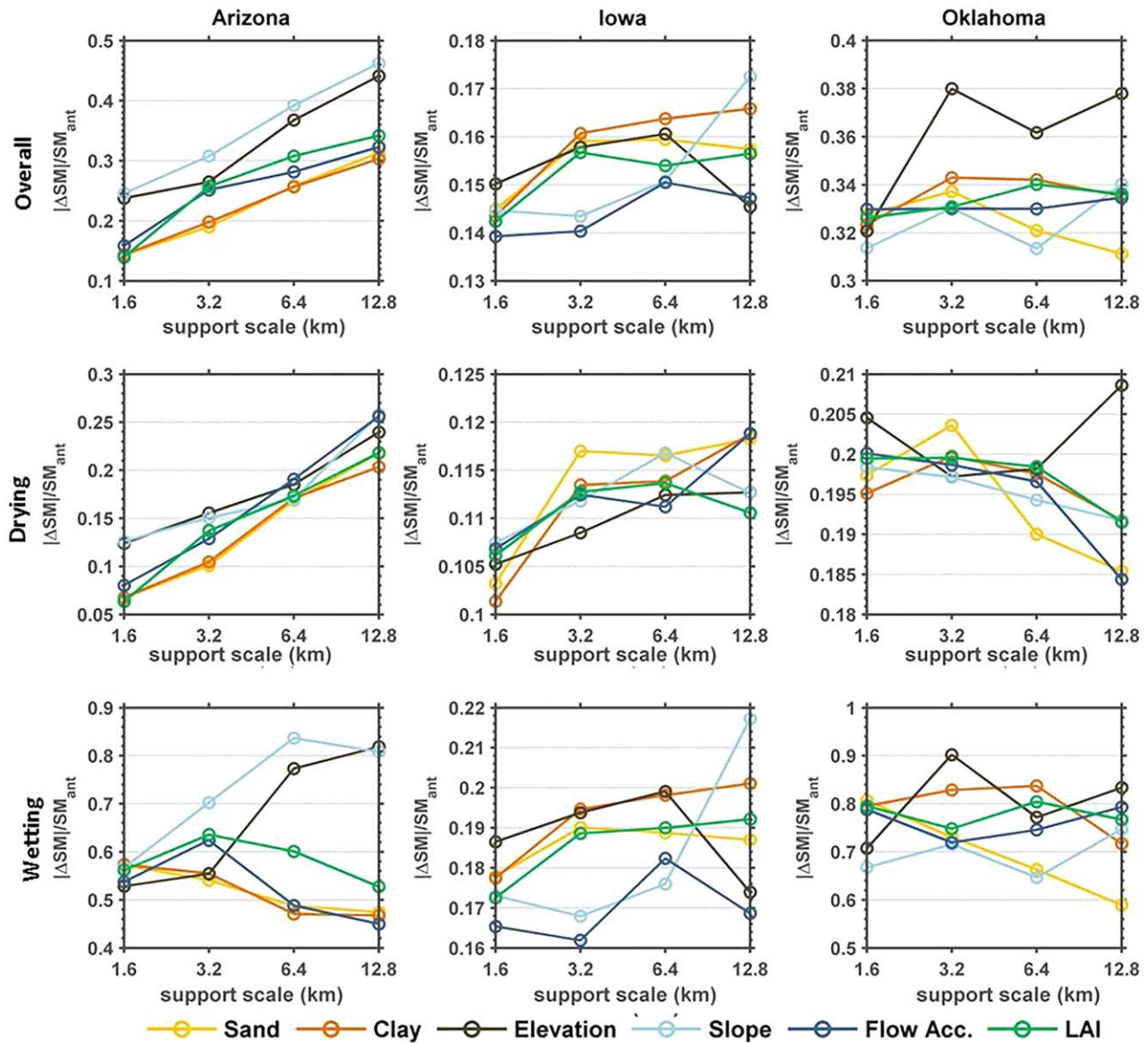


Figure 9. Mean $\Delta SM_{norm,t}$ observed in regions where pattern matches with % sand, % clay, elevation, slope, flow accumulation, and LAI are observed for (a) all pixels, (b) drying pixels, and (c) wetting pixels.

flow into the soil through stem flow. The association between spatial LAI patterns and moisture was significant in all three regions. The percentage of pattern matches, show a general increasing trend with scale. In Oklahoma, vegetation becomes the most spatially dominant factor at support scale 3.2 km and above.

Iowa is an agricultural region with crops of different LAI. The significance of vegetation in Iowa is slightly more in the drying pixels as compared to wetting pixels. This implies higher differences in evapotranspiration losses because of crops with different LAI as opposed to differential interception of rain water by the varied plant types (Figures 8b and 8c). Similarly, Oklahoma which is mostly grassland region with some agriculture also displays a higher contribution of vegetation in the drying scenario. In the sparsely vegetated Arizona, the trend is opposite with higher vegetation contribution for wetting pixels. It signifies a dominance of processes like interception and leaf evaporation from intercepted water. The land cover in Arizona comprises of sparse desert shrubland, grassland, and few crops [Yilmaz *et al.*, 2008]. The spatial heterogeneity in vegetation types creates differences in intercepted water and its contribution to soil moisture dynamics.

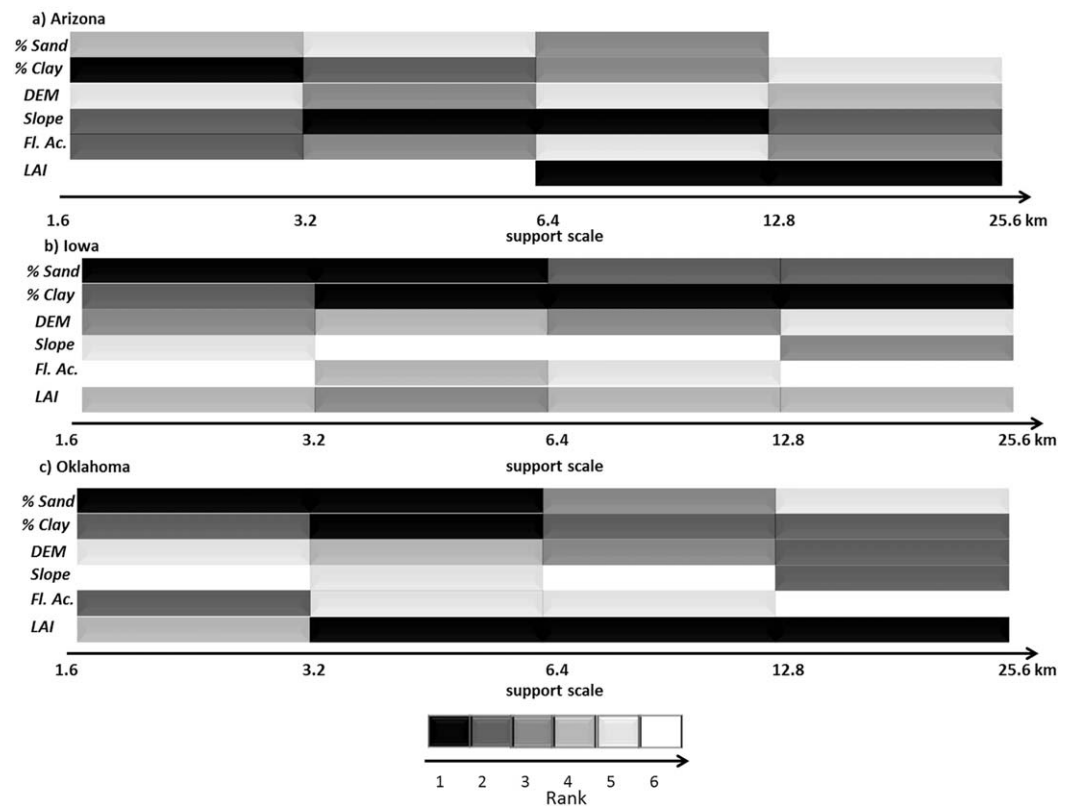


Figure 10. Hierarchy of effect of biophysical factors on near-surface soil moisture distribution.

4.2.2. Effect of Physical Factors on Magnitude of Soil Moisture Redistribution, $M_{f,s}$

Figure 9 shows the mean of the absolute values of $\Delta SM_{norm,t}$ (equation (12)) observed in regions where the pattern matches between various biophysical factors and $\Delta SM_{norm,t}$ were observed. These values reflect the mean soil moisture changes occurring at the location where a biophysical factor was observed to control soil moisture redistribution. Large values would indicate greater contribution of the biophysical factor in affecting soil moisture changes. The range and maximum value of $\Delta SM_{norm,t}$ were higher for the wetting pixels than the drying pixels (Figure 9). The higher range of the $\Delta SM_{norm,t}$ during wetting can be attributed to higher variability in rainfall input to the system which leads to higher variations in soil moisture. Overall, Arizona, and Oklahoma showed larger ranges of $\Delta SM_{norm,t}$ whereas they were smaller in Iowa. This partly occurred since there were no heavy precipitation events in Iowa and also the moisture conditions in Iowa did not become extremely dry (Figure 3). It was also observed that topography showed significantly greater contribution in Arizona. Mixed effects were observed in Iowa with soil and topography showing higher ΔSM_{norm} than other factors at different scales. Likewise in Oklahoma, topography and soil showed higher ΔSM_{norm} . These results also reveal that the physical factors which had lower spatial influence (in terms of areal extent) on soil moisture redistribution (Figure 8), may have greater influence on the amount

Table 3. Median of the Antecedent Moisture Values of the Regions at Which a Pattern Match Between the Given Physical Factors and Moisture Redistribution Was Observed Median Antecedent Moisture

Support scale	1.6 km	3.2 km	6.4 km	12.8 km
ARIZONA				
Soil (Clay)	0.021	0.073	0.093	0.076
Topography (Elevation)	0.099	0.100	0.085	0.060
Vegetation (LAI)	0.020	0.068	0.078	0.077
IOWA				
Soil (Clay)	0.214	0.208	0.210	0.210
Topography (Elevation)	0.215	0.212	0.202	0.203
Vegetation (LAI)	0.209	0.205	0.205	0.204
OKLAHOMA				
Soil (Sand)	0.170	0.180	0.170	0.230
Topography (Elevation)	0.180	0.180	0.170	0.190
Vegetation (LAI)	0.170	0.170	0.150	0.180

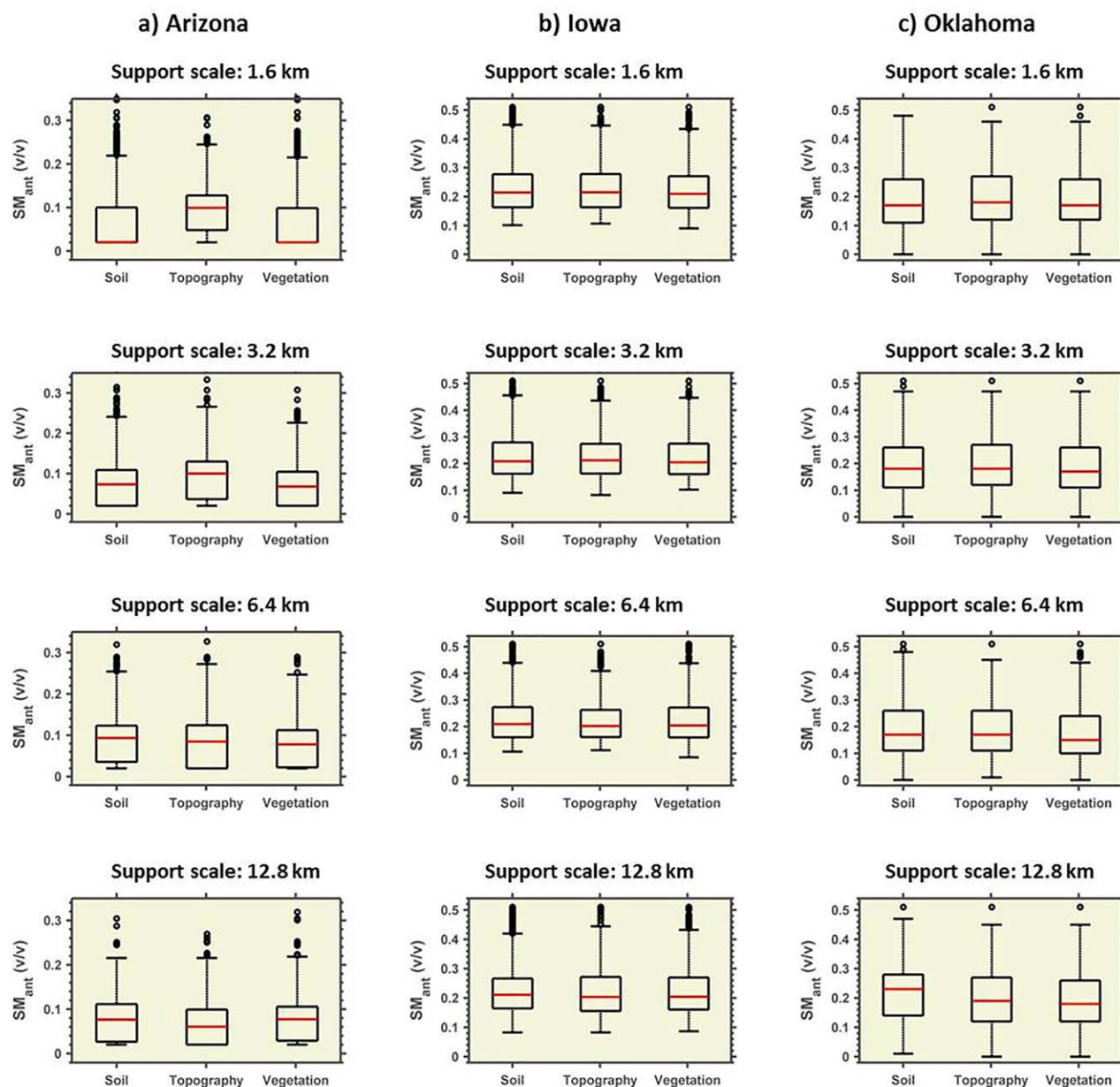


Figure 11. SM_{ant} distribution of regions where soil, topography, and vegetation are dominant.

of moisture redistribution that takes place and can thus; greatly alter the water budget in the limited spatial regions where they are important. It is worthwhile to note that contrary to its spatial influence, the magnitude of vegetation effect was typically low in all three regions.

4.3. Overall Ranking Scheme

In order to characterize the overall effects of the physical factors on soil moisture distribution and provide a general guideline for the three hydroclimates, the physical factors were ranked based on the magnitude of controls (Figure 9a) and areal extent of controls (Figure 8a). Equal weight was given to both the components and the hierarchy of physical factors on defining near-surface soil moisture distribution was evaluated. Results are depicted for the three study regions in Figure 10. A lower numerical rank implies greater overall control of the physical factor on soil moisture at a particular scale. In Arizona, soil (or specifically % clay), is the most dominant land-surface factor at the 1.6–3.2 km support scale range, while topography

Table 4. Significance Results of Wilcoxon Rank Sum (WRS) Test Marking the Existence of a Threshold Value^a

Region/Scale	1.6 km	3.2 km	6.4 km	12.8 km
Soil and Topography				
Arizona	x	x	x	X
Iowa				
Oklahoma	x	x	x	X
Soil and Vegetation				
Arizona	x		x	
Iowa				
Oklahoma		x	x	X
Topography and Vegetation				
Arizona	x	x	x	X
Iowa				
Oklahoma	x	x	x	

^a"x" represents a WRS result significant at 95%.

(slope) and vegetation (LAI) become more dominant at 3.2–12.8 km and 6.4–25.6 km support scale range, respectively. Soil remains the most dominating factor in Iowa consistently with % sand being most dominant at the 1.6–3.2 km support scale range beyond which % clay becomes most dominant. As in Arizona, we observe that soil (% sand) is dominant at the relatively finer support scales (1.6–6.4 km) while vegetation becomes most important between 3.2 and 25.6 km support scale range in Oklahoma. Topography exerts little dominance at the finer scales and moderate dominance at the relatively coarse support scales.

4.4. Investigating Antecedent Moisture-Based Thresholds

Processes that control moisture movement in the soil surface are influenced by the amount of water in the domain and the heterogeneity comprised of different biophysical factors in the domain. In order to investigate the presence of threshold antecedent moisture values at which different biophysical factors (and thus related hydrologic processes) become dominant, the antecedent soil moisture conditions of the pixels at which different biophysical factors become dominant (pattern matched locations) were compared using the Wilcoxon rank sum (WRS) tests. WRS test is the nonparametric equivalent of the *t*-test and assesses a difference in the distribution of the ranks of the ordered observations as opposed to their actual values. The physical factors which showed maximum overall control (Figure 10) on moisture redistribution values were chosen to represent soil, topography, and vegetation attributes. The median values for the same attributes are provided in Table 3. Figure 11 shows the antecedent soil moisture distribution of the regions where the particular biophysical factor was found important while the WRS significance results are provided in Table 4. We observe that there are statistically significant differences in the antecedent moisture distribution of topography when compared to soil and vegetation in Arizona whereas in Iowa, there are no statistically significant differences/thresholds observed. In Oklahoma, the effect of soil is statistically significantly different from topography at all scales and from vegetation at 3.2–25.6 km support scale range. However, median moisture difference (Table 3) that is less than the standard error of retrievals may reflect retrieval errors and not true thresholds. The difference between the median values of antecedent moisture values of the regions where different biophysical factors dominate is relatively small in Oklahoma (<0.03 v/v) and within the error range. In Arizona on the other hand, we observe that differences are more than the remote sensing measurement error (>0.014 v/v) [Bindlish et al., 2008]. This implies that at remote sensing footprint scales, antecedent moisture-based thresholds at which the controls switch from one land-surface factor to the other may be effectively identified only in some regions.

5. Conclusions

In this study, nondecimated wavelet analysis was used to assess the influence of land-surface based physical factors, namely, soil (% sand, % clay), topography (elevation, slope, flow accumulation), and vegetation (leaf area index) on soil moisture redistribution at remote sensing footprint scales varying from 1.6 to 25.6 km. The contribution of the different biophysical factors was computed in terms of areal extent of influence of the biophysical factor and the magnitude of moisture redistribution associated with it to define their hierarchical control on soil moisture dynamics. The hierarchy was defined for coarse spatial support scales but fine (daily) temporal spacing scales which are typical of remotely sensed soil moisture data. The influence of biophysical factors on soil moisture redistribution at remote sensing footprints varied across different hydroclimates and scales. Soil is the dominant physical factor in Iowa across all scales whereas the topography and vegetation are the dominant physical controls in Arizona starting at 3.2 and 6.4 km, respectively. In Oklahoma, on the other hand, soil is the dominant factor at 1.6–3.2 km but vegetation has a more significant effect at coarser scales. The effect of hydroclimate was also identifiable in the soil attributes

dominating the soil moisture dynamics. The near-surface soil moisture dynamics in Arizona (semiarid) can be more attributed to the clay content which is effective limiting parameter for evaporation whereas in the humid Oklahoma, % sand (effectively limiting drainage) was the dominant attribute of soil. Antecedent moisture-based thresholds at which the effect of different physical factors becomes significant were also found to be hydroclimate specific and found to exist only in Arizona.

The study was conducted under the assumption that the soil moisture retrievals at 800 m are accurate. This assumption may cause some uncertainty in the evaluated threshold values. This study is limited by the regional extent, hydroclimates and also time period (growing season) analyzed. However, it provides a direction for understanding hydroclimate-based dependence of near-surface soil moisture on physical factors. These findings can assist in developing more effective physically based soil moisture scaling schemes and in the improvement of processes in large-scale hydrological models.

Acknowledgments

We would like to thank the anonymous reviewers and editors for their valuable suggestions. We also acknowledge the funding support of NASA Earth and Space Science Fellowship (NNX13AN64H), NASA THPs (NNX08AF55G and NNX09AK73G), and NSF (DMS-09-34837) grants. The soil moisture data set for Oklahoma was obtained via personal communication with Michael H. Cosh (Michael.cosh@ars.usda.gov) at United States Department of Agriculture. The soil elevation (1 arc second resolution), LAI (1 km resolution), and soil moisture data sets for Iowa and Arizona used in this study can be accessed from the links provided below: http://www.soilinfo.psu.edu/index.cgi?soil_data&conus, <http://viewer.nationalmap.gov/viewer/>, <http://reverb.echo.nasa.gov/reverb/>, and http://nsidc.org/data/amr_validation/soil_moisture/index.html

References

- Ackerman, E. A. (1941), The Köppen classification of climates in North America, *Geogr. Rev.*, 31(1), 105–111.
- Bindlish, R., T. J. Jackson, A. J. Gasiewski, M. Klein, and E. G. Njoku (2006), Soil moisture mapping and AMSR-E validation using the PSR in SMEX02, *Remote Sens. Environ.*, 103(2), 127–139, doi:10.1016/j.rse.2005.02.003.
- Bindlish, R., et al. (2008), Aircraft based soil moisture retrievals under mixed vegetation and topographic conditions, *Remote Sens. Environ.*, 112(2), 375–390, doi:10.1016/j.rse.2007.01.024.
- Blöschl, G., and M. Sivapalan (1995), Scale issues in hydrological modelling: A review, *Hydrol. Processes*, 9(3–4), 251–290.
- Burt, T. P., and D. P. Butcher (1985), Topographic controls of soil moisture distributions, *J. Soil Sci.*, 36(3), 469–486.
- Coleman, M. L., and J. D. Niemann (2013), Controls on topographic dependence and temporal instability in catchment-scale soil moisture patterns, *Water Resour. Res.*, 49, 1625–1642, doi:10.1002/wrcr.20159.
- Cosh, M. H., and W. Brutsaert (1999), Aspects of soil moisture variability in the Washita'92 study region, *J. Geophys. Res.*, 104(D16), 19,751–19,757.
- Crow, W. T., and E. F. Wood (1999), Multi-scale dynamics of soil moisture variability observed during SGP'97, *Geophys. Res. Lett.*, 26(23), 3485–3488.
- Das, N. N., and B. P. Mohanty (2008), Temporal dynamics of PSR-based soil moisture across spatial scales in an agricultural landscape during SMEX02: A wavelet approach, *Remote Sens. Environ.*, 112(2), 522–534, doi:10.1016/j.rse.2007.05.007.
- Farnsworth, R. K., E. S. Thompson, and E. L. Peck (1982), Evaporation Atlas for the Contiguous 48 United States: US Department of Commerce, National Oceanic and Atmospheric Administration, National Weather Service, NOAA Technical Report NWS 33, 35pp.
- Gaur, N., and B. P. Mohanty (2013), Evolution of physical controls for soil moisture in humid and subhumid watersheds, *Water Resour. Res.*, 49, 1244–1258, doi:10.1002/wrcr.20069.
- Gesch, D., G. Evans, J. Mauck, J. Hutchinson, and W. J. Carswell Jr. (2009), The National Map—Elevation, *U.S. Geol. Surv. Fact Sheet 2009-3053*, 4 pp.
- Gesch, D. B., M. J. Oimoen, and G. A. Evans (2014), Accuracy assessment of the U.S. Geological Survey National Elevation Dataset, and comparison with other large-area elevation datasets—SRTM and ASTER, *U.S. Geol. Surv. Open File Rep.*, 2014–1008, 10 pp, doi:10.3133/ofr20141008.
- Goulden, M. L., R. G. Anderson, R. C. Bales, A. E. Kelly, M. Meadows, and G. C. Winston (2012), Evapotranspiration along an elevation gradient in California's Sierra Nevada, *J. Geophys. Res.*, 117, G03028, doi:10.1029/2012JG002027.
- Green, T. R., and R. H. Erskine (2011), Measurement and inference of profile soil-water dynamics at different hillslope positions in a semiarid agricultural watershed, *Water Resour. Res.*, 47, W00H15, doi:10.1029/2010WR010074.
- Ivanov, V. Y., S. Faticchi, G. D. Jenerette, J. F. Espeleta, P. A. Troch, and T. E. Huxman (2010), Hysteresis of soil moisture spatial heterogeneity and the “homogenizing” effect of vegetation, *Water Resour. Res.*, 46, W09521, doi:10.1029/2009WR008611.
- Jackson, T. J., D. M. Le Vine, A. Y. Hsu, A. Oldak, P. J. Starks, C. T. Swift, J. D. Isham, and M. Haken (1999), Soil moisture mapping at regional scales using microwave radiometry: The southern great plains hydrology experiment, *IEEE Trans. Geosci. Remote Sens.*, 37(5), 2136–2151, doi:10.1109/36.789610.
- Jackson, T. J., R. Bindlish, M. Klein, A. J. Gasiewski, and E. G. Njoku (2003), Soil moisture retrieval and AMSR-E validation using an airborne microwave radiometer in SMEX02, in *Geoscience and Remote Sensing Symposium, 2003. IGARSS'03. Proceedings. 2003 IEEE International*, vol. 1, pp. 401–403, IEEE, doi:10.1109/IGARSS.2003.1293789.
- Jawson, S. D., and J. D. Niemann (2007), Spatial patterns from EOF analysis of soil moisture at a large scale and their dependence on soil, land-use, and topographic properties, *Adv. Water Resour.*, 30(3), 366–381, doi:10.1016/j.advwatres.2006.05.006.
- Joshi, C., and B. P. Mohanty (2010), Physical controls of near-surface soil moisture across varying spatial scales in an agricultural landscape during SMEX02, *Water Resour. Res.*, 46, W12503, doi:10.1029/2010WR009152.
- Katzberg, S. J., O. Torres, M. S. Grant, and D. Masters (2006), Utilizing calibrated GPS reflected signals to estimate soil reflectivity and dielectric constant: Results from SMEX02, *Remote Sens. Environ.*, 100(1), 17–28.
- Kim, G., and A. P. Barros (2002), Space-time characterization of soil moisture from passive microwave remotely sensed imagery and ancillary data, *Remote Sens. Environ.*, 81, 393–403.
- Kumar, P., and E. Foufoula-Georgiou (1993), A multicomponent decomposition of spatial rainfall fields: 1. Segregation of large- and small-scale features using wavelet transforms, *Water Resour. Res.*, 29(8), 2515–2532, doi:10.1029/93WR00548.
- Kumar, P., and E. Foufoula-Georgiou (1997), Wavelet analysis for geophysical applications, *Rev. Geophys.*, 35(4), 385–412.
- Logsdon, S. D. (2015), Event- and site-specific soil wetting and seasonal change in amount of soil water, *Soil Sci. Soc. Am. J.*, 79(3), 730–741.
- Mahrt, L. (1991), Eddy asymmetry in the shear heated boundary layer, *J. Atmos. Sci.*, 48, 471–492.
- Miller, D. A., and R. A. White (1998), A conterminous United States multi-layer soil characteristics data set for regional climate and hydrology modeling, *Earth Interact.*, 2. [Available at <http://EarthInteractions.org>.]
- Mohanty, B. P., and T. H. Skaggs (2001), Spatiotemporal evolution and time-stable characteristics of soil moisture within remote sensing footprints with varying soil, slope, and vegetation, *Adv. Water Resour.*, 24(9), 1051–1067, doi:10.1016/S0309-1708(01)00034-3.

- Mohanty, B. P., and J. Zhu (2007), Effective hydraulic parameters in horizontally and vertically heterogeneous soils for steady-state land-atmosphere interaction, *J. Hydrometeorol.*, *8*, 715–729, doi:10.1175/JHM606.1.
- Mohanty, B. P., T. H. Skaggs, and J. S. Famiglietti (2000a), Analysis and mapping of field-scale soil moisture variability using high-resolution, ground-based data during the Southern Great Plains 1997 (SGP97) Hydrology Experiment, *Water Resour. Res.*, *36*(4), 1023–1031, doi:10.1029/1999WR900360.
- Mohanty, B. P., J. S. Famiglietti, and T. H. Skaggs (2000b), Evolution of soil moisture spatial structure in a mixed vegetation pixel during the Southern Great Plains 1997 (SGP97) Hydrology Experiment, *Water Resour. Res.*, *36*(12), 3675–3686, doi:10.1029/2000WR900258.
- Nachshon, U., N. Weisbrod, M. I. Dragila, and A. Grader (2011), Combined evaporation and salt precipitation in homogeneous and heterogeneous porous media, *Water Resour. Res.*, *47*, W03513, doi:10.1029/2010WR009677.
- NASA Land Processes Distributed Active Archive Center (2001), (LP DAAC) MODIS (LAI/FPAR- 4 day composite), USGS/Earth Resour. Observ. and Sci. (EROS) Cent., Sioux Falls, S. D.
- Oldak A, T. J. Jackson, and Y. Pachepsky (2002), Using GIS in passive microwave soil moisture mapping and geostatistical analysis, *Int. J. Geogr. Inform. Sci.*, *16*(7), 681–698, doi:10.1080/13658810210149407.
- Peel, M. C., B. L. Finlayson, and T. A. McMahon (2007), Updated world map of the Köppen-Geiger climate classification, *Hydrol. Earth Syst. Sci. Discuss.*, *4*(2), 439–473.
- Percival, D. B., and A. T. Walden (2000), *Wavelet Methods for Time Series Analysis, Cambridge Series in Statistical and Probabilistic Mathematics*, Cambridge University Press.
- Percival, D. B., S. M. Lennox, Y.-G. Wang, and R. E. Darnell (2011), Wavelet-based multiresolution analysis of Wivenhoe Dam water temperatures, *Water Resour. Res.*, *47*, W05552, doi:10.1029/2010WR009657.
- R Core Team (2013), R: A language and environment for statistical computing. R Found. for Stat. Comput., Vienna, Austria. [Available <http://www.R-project.org/>]
- Richards, L. A. (1931), Capillary conduction of liquids through porous mediums, *Physics*, *1*(5), 318–333.
- Ryu, D., and J. S. Famiglietti (2006), Multi-scale spatial correlation and scaling behavior of surface soil moisture, *Geophys. Res. Lett.*, *33*, L08404, doi:10.1029/2006GL025831.
- Ryu, D., T. J. Jackson, R. Bindlish, D. M. Le Vine, and M. Haken (2010), Soil moisture retrieval using a two-dimensional L-band synthetic aperture radiometer in a semiarid environment, *IEEE Trans. Geosci. Remote Sens.*, *48*(12), 4273–4284.
- Si, B. C. (2008), Spatial scaling analyses of soil physical properties: A review of spectral and wavelet methods, *Vadose Zone J.*, *7*(2), 547–562, doi:10.2136/vzj2007.0040.
- Si, B. C., and T. B. Zeleke (2005), Wavelet coherence analysis to relate saturated hydraulic properties to soil physical properties, *Water Resour. Res.*, *41*, W11424, doi:10.1029/2005WR004118.
- Strand, E. K., Smith, A. M., Bunting, S. C., Vierling, L. A., Hann, D. B., & Gessler, P. E. (2006), Wavelet estimation of plant spatial patterns in multitemporal aerial photography, *Int. J. Remote Sens.*, *27*(10), 2049–2054. doi:10.1080/01431160500444764.
- Teuling, A. J., F. Hupet, R. Uijlenhoet, and P. A. Troch (2007), Climate variability effects on spatial soil moisture dynamics, *Geophys. Res. Lett.*, *34*, L06406, doi:10.1029/2006GL029080.
- Western, A. W., R. B. Grayson, G. Blöschl, G. R. Willgoose, and T. A. McMahon (1999), Observed spatial organization of soil moisture and its relation to terrain indices, *Water Resour. Res.*, *35*(3), 797–810.
- Whitcher, B. (2012), waveslim: Basic wavelet routines for one-, two- and three-dimensional signal processing. R package version 1.7.1. [Available <http://CRAN.R-project.org/package=waveslim>.]
- Wu, S., J. Li, and G. H. Huang (2008), A study on DEM-derived primary topographic attributes for hydrologic applications: Sensitivity to elevation data resolution, *Appl. Geogr.*, *28*(3), 210–223, doi:10.1016/j.apgeog.2008.02.006.
- Yilmaz, M. T., E. R. Hunt, L. D. Goins, S. L. Ustin, V.C. Vanderbilt, and T. J. Jackson (2008), Vegetation water content during SMEX04 from ground data and Landsat 5 Thematic Mapper imagery, *Remote Sens. Environ.*, *112*(2), 350–362.
- Zhu, J., and B. P. Mohanty, (2002a), Spatial averaging of van Genuchten hydraulic parameters for steady-state flow in heterogeneous soils, *Vadose Zone J.*, *1*(2), 261–272.
- Zhu, J., and B. P. Mohanty (2002b), Upscaling of soil hydraulic properties for steady state evaporation and infiltration, *Water Resour. Res.*, *38*(9), 1178, doi:10.1029/2001WR000704.